

Atomistic simulation of dopant substitution in $\text{YBa}_2\text{Cu}_3\text{O}_7$

M. S. Islam* and R. C. Baetzold

Research Laboratories, Eastman Kodak Company, Rochester, New York 14650-2021

(Received 6 June 1989)

A wide range of cation dopant substitutions in $\text{YBa}_2\text{Cu}_3\text{O}_7$ is investigated using computer-simulation techniques. Attention is focused on site selectivity and possible charge-compensation mechanisms. The calculated solution energies show strong systematic variations as a function of dopant ion radius. Our results suggest that Ni^{2+} , Zn^{2+} , and Cd^{2+} preferentially substitute for Cu^{2+} in the plane, whereas the alkaline-earth ions Ca^{2+} and Sr^{2+} dissolve in the crystal at the Ba^{2+} site. We consider two extreme cases of localization for trivalent dopant substitution of copper with the compensating oxygen interstitial. The calculations predict that Al^{3+} and Fe^{3+} occupy the Cu(2) site for the delocalized model and the Cu(1) site for the more localized model. Substitution of rare-earth ions, such as La^{3+} , is energetically most favorable at the barium site. Correlations between particular bond distances and T_c are also discussed.

I. INTRODUCTION

Numerous investigations¹⁻¹⁹ have been made on the effects of incorporating dopants into the oxide superconductor $\text{YBa}_2\text{Cu}_3\text{O}_7$. A greater understanding of the superconducting and structural properties of the doped material is important, not only to elucidate the nature of possible mechanisms, but also because these potentially deleterious phases are commonly formed during synthesis of composites and thin films.

In the case of the complete substitution of Y^{3+} by the magnetic and isoelectronic rare-earth ions,^{1,15} that is, $R\text{Ba}_2\text{Cu}_3\text{O}_7$ (where $R = \text{La, Nd, Sm, Eu, Gd, Ho, Er, and Lu}$), there is no substantial change in the superconducting transition temperature (T_c). The $R\text{Ba}_2\text{Cu}_3\text{O}_7$ superconducting materials are also found to crystallize into the same orthorhombic structure²⁰⁻²² as $\text{YBa}_2\text{Cu}_3\text{O}_7$, which is shown in Fig. 1, indicating our site notation. Similarly, when barium is replaced by other alkaline-earth cations¹⁷ the structure remains essentially identical, with a general trend towards a continuous decrease in T_c . However, for addition of 3d transition elements, which occupy the copper sites, T_c is depressed considerably with the magnitude of the effect dependent upon the concentration and the character of the dopant ion.^{2,3,5,7,11-14,16} Most notably substitution of the closed-shell ($3d^{10}$) Zn^{2+} produces an anomalously large T_c suppression. In addition, some non-magnetic ions, such as Al^{3+} and Ga^{3+} , that replace copper are found to reduce T_c with increasing substitution.⁴⁻⁶

An important structural feature of $\text{YBa}_2\text{Cu}_3\text{O}_7$ is the existence of two crystallographically independent copper sites, consisting of square-planar CuO_3 chains, [Cu(1)], and square-pyramidal CuO_2 planes in the a - b plane, [Cu(2)]. The relative importance and specific roles of planes versus chains are still debatable. In evaluating the influence of substituting ions into $\text{YBa}_2\text{Cu}_3\text{O}_7$ it is apparent that the precise lattice location is important. Experimentally, in some cases, the preferred site for dopant

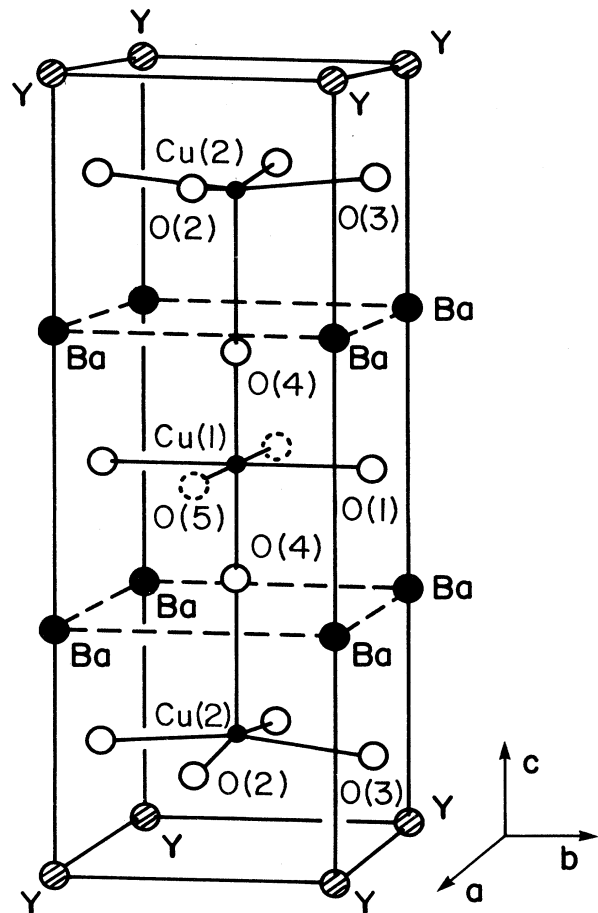


FIG. 1. Unit cell of the $\text{YBa}_2\text{Cu}_3\text{O}_7$ orthorhombic crystal structure (after Refs. 20-22), indicating our site notation.

ion substitution has not been clearly established, in particular for the Cu(1) and Cu(2) positions. This partly arises from difficulties in performing accurate experimental work on samples whose oxygen stoichiometry may be poorly characterized.

Recently, theoretical methods have been developed that successfully describe properties of local defects in oxide materials.^{23–25} These methods, though conceptually simple, have demonstrated impurity effects in relation to ion size, charge, and compensation mechanisms. Based on these examples, the methods have been extended to ceramic oxide superconductors, where good descriptions of structural and defect properties, and phonon dispersion curves have been found. We now systematically extend our recent investigations of ionic and electronic defects in $\text{YBa}_2\text{Cu}_3\text{O}_7$ (Ref. 26) and the La_2CuO_4 system,²⁷ by examining the energetics of dopant incorporation into the $\text{YBa}_2\text{Cu}_3\text{O}_7$ material. In our previous study²⁶ of $\text{YBa}_2\text{Cu}_3\text{O}_7$, a two-body potential model was developed that successfully reproduced the crystal structure and correctly predicted the most favorable site for oxygen vacancies. This paper focuses on the preferential site location of substituting ions within the copper, yttrium, and barium sublattices and the possible correlation with ionic radius. We note that the simulation methods employed are well suited to probe the energetics of dopant substitution as they model, accurately, the relaxation of lattice atoms surrounding the defect species.

II. THEORETICAL METHODS

Since more detailed descriptions of the methods and their applications to other systems are presented elsewhere,^{23,25} we will give a brief account of the model used. The simulations are based on a Born model representation of polar solids, which requires specification of two-body, central force potentials representing the short-range interactions. The interatomic potentials are commonly described by an analytical function of the Buckingham form:

$$\phi_{ij}(r_{ij}) = A_{ij} \exp(-r_{ij}/\rho_{ij}) - C_{ij}/r_{ij}^6, \quad (1)$$

where the exponential term represents the Pauli repulsion that arises from overlapping wave functions on different atoms. It is usual to associate the attractive r^{-6} term with van der Waals forces. In practice, however, this term will include contributions from other attractive forces such as small covalent terms. Without a satisfactory treatment of ionic polarization it is not possible to describe correctly the response of the crystal to the electrostatic perturbation caused by a charge defect. Polarization is simulated effectively by the shell model,²⁸ which describes the ionic dipole in terms of the displacement of a massless electron shell from a core in which the mass is concentrated; the core and shell being coupled by an isotropic harmonic spring. Note that the non-Coulombic forces act only between shells, thus including the vital coupling between short-range forces and polarization by the remainder of the lattice. This coupling is of importance in the simulation of both elastic and dielectric properties of the crystal, and was previously neglected in

simpler point-ion models. Energy minimization of the perfect lattice is achieved using an iterative procedure, involving first and second derivatives of the lattice energy with respect to internal and bulk strains. An important feature of the defect calculations concerns the determination of the relaxations of lattice ions surrounding the defect. These are calculated by an explicit energy minimization for a spherical region immediately surrounding the defect (region I), that contains typically 200 ions. The response of the remainder of the crystal (region II) is obtained using a continuum treatment based on the Mott-Littleton approximation,²⁹ since the forces exerted by the defect in the more distant lattice are relatively weak. These simulation techniques are incorporated into the CASCADE (Ref. 30) and HADES (Ref. 31) computer codes.

In attempting to assess the relative energetics of dopant substitution we use the same potentials for $\text{YBa}_2\text{Cu}_3\text{O}_7$ as in the previous treatment of Baetzold.²⁶ As in this latter study, all copper ions are considered in the $2+$ charge state, with the hole uniformly distributed on the oxygen ions at O(1) and O(4) positions. Alternatively charge distribution models²⁶ were not as successful at either reproducing the structure or deriving stable potentials. With regard to the dopant ion-host ion interactions, the potentials were derived empirically by fitting to observed crystal properties of the relevant binary oxides, and have been successfully applied to a study of impurities in BaTiO_3 (Ref. 32). The perfect-lattice potentials employed for $\text{YBa}_2\text{Cu}_3\text{O}_7$ are based on the fully ionic model. The validity of using such potentials is supported by the success of defect calculations for a wide range of oxide materials.^{32–35} Moreover, support is provided first by the close agreement obtained between calculated and experimental bond distances²⁶ of $\text{YBa}_2\text{Cu}_3\text{O}_7$; the largest deviation is less than 0.03 Å. Second, the potential model yields calculated phonon dispersion curves that exhibit full stability; that is, no imaginary frequencies are observed.³⁶ It should be stressed, as argued previously,^{37,38} that the validity of a potential model is assessed primarily by its ability to reproduce experimental crystal properties. Indeed, in practice it is found that models based on formal charges work well in simulating physical properties even for some semicovalent compounds, such as silicates.³⁵ Note that with additional experimental data, particularly dielectric and elastic constants, it will be possible to either test or further refine our potential model for $\text{YBa}_2\text{Cu}_3\text{O}_7$. With regard to calculations presented in this paper, we should add that most substitution experiments are carried out at elevated temperatures where the materials exhibit nonmetallic behavior. For such systems the techniques have been shown to be reliable.

III. RESULTS AND DISCUSSION

The principal dopants or impurities in $\text{YBa}_2\text{Cu}_3\text{O}_7$ are divalent and trivalent cations. We consider both types of dopant substituting on the Cu^{2+} , Y^{3+} , and Ba^{2+} sublattices. Our discussion will ignore the effect of defect interactions leading to possible aggregation; the results presented therefore refer to systems at very low dopant

concentration. The simulation approach is based on the calculation of the energetics of dissolution in the oxide. In the examination of preferred sites of substitution it is assumed that these can be predicted on energetic argument alone; that is, we neglect the contribution of defect entropies to the free energy of solution. Given this assumption, the energies of solution are obtained by combining appropriate cohesive energies with lattice energy terms accompanying the formation of the substitutional species.

A. Substitution for copper

We first consider the dissolution of divalent impurities into the Cu^{2+} sublattice, which can be represented by the defect equation:



(Note that in the Kroger-Vink notation³⁹ used in this paper, vacancies, interstitials, and substitutionals are denoted as V_{Cu} , Cu_i , and M_{Cu} , respectively). Since this mode of solution involves isovalent substitution, charge compensation is not necessary. This is consistent with thermogravimetric data,⁵ which find no significant change in oxygen stoichiometry with increasing divalent (Ni, Zn) doping. The calculated energies of solution, ΔE , for the two nonequivalent copper sites are listed in Table I, where our sign convention is such that a positive value indicates an endothermic process.

The calculations suggest that the transition-metal cations Fe^{2+} , Co^{2+} , Ni^{2+} , Zn^{2+} , and Cd^{2+} preferentially substitute for $\text{Cu}(2)$. Most notably, the highly favorable solution energies for NiO and ZnO are in line with the observation that these oxides dissolve readily in $\text{YBa}_2\text{Cu}_3\text{O}_7$. The results in Table I generally agree with diffraction studies^{5,7} that find Ni^{2+} and Zn^{2+} on the $\text{Cu}(2)$ plane. Note that experimentally, Fe and Co are considered to be in the $3+$ charge state, which will be examined later. It should also be noted that as well as cation substitution, there is also the possibility of dopants entering the crystal lattice at interstitial positions, which is still under investigation.

It has been proposed that the $\text{Cu}(2)$ plane plays a more important role in superconductivity mechanism than the

$\text{Cu}(1)$ chain. This is supported by the observation of high- T_c superconductivity in the Tl- and Bi-based systems, which contain copper-oxygen planes but no chains. The substitution of $\text{Cu}(2)$ is, therefore, expected to produce a significant change in transition temperature (T_c) with increasing dopant concentration. Indeed, large depressions in T_c have been observed^{2,3,5,7} for transition-metal ion incorporation into $\text{YBa}_2\text{Cu}_3\text{O}_7$. Our results also clearly indicate the importance of the $\text{Cu}(2)$ planes.

In Fig. 2(a) the calculated energies of solution are plot-

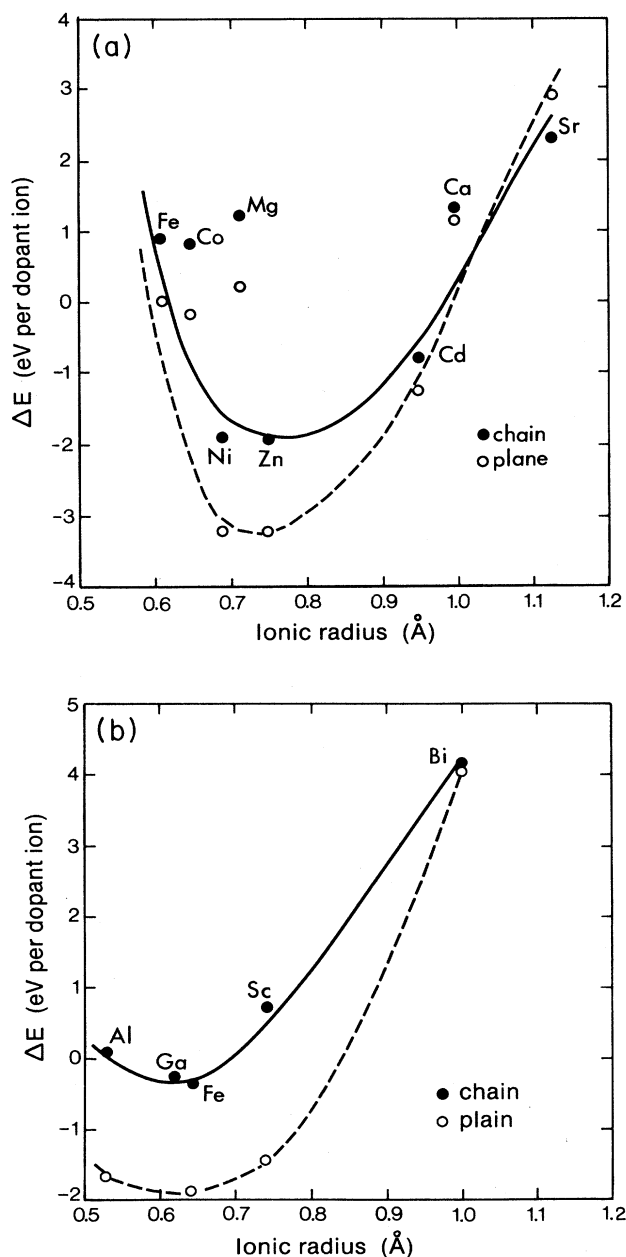


TABLE I. Calculated energies of solution (positive values indicate an endothermic process) (in eV per dopant ion) for divalent cation substitution for copper.

MO	$MO + \text{Cu}_{\text{Cu}}^x = M_{\text{Cu}}^x + \text{CuO}$	
	$\Delta E_{\text{Cu}(1)}$	$\Delta E_{\text{Cu}(2)}$
MgO	1.20	0.18
CaO	1.28	1.15
SrO	2.28	2.94
FeO	0.91	0.02
CoO	0.85	-0.10
NiO	-1.86	-3.19
ZnO	-1.96	-3.18
CdO	-0.82	-1.23

FIG. 2. Calculated energies of solution as a function of dopant ion radius for copper substitution (a) divalent ions, (b) trivalent ions. The lines are guides to the eye.

ted versus the ionic radius of the dopant ion; a strong correlation between the two is found, with an energy minimum observed at Ni^{2+} . Very similar behavior has been observed from impurity studies³² of the perovskite-structured BaTiO_3 . Such variation with dopant ion size is explained in terms of the relaxation of the surrounding ions, and suggests that changes in local structural ordering are important in the observed depressions in T_c as opposed to long-range effects. In general, various mechanisms have been proposed to explain the reduction in T_c with dopant incorporation. These include magnetic pair breaking, changes in oxygen stoichiometry, orthorhombic-tetragonal phase transition, local disordering effects, and reduction in the carrier concentration.

The simulation program used in this study provides detailed information on the relaxed positions of host-lattice ions in the immediate vicinity of the dopant ion. The most significant movements are illustrated in Fig. 3, for the example of Zn^{2+} replacing $\text{Cu}(2)$. This indicates a displacement of the dopant ion of 0.05 \AA along the c -axis direction, away from the $\text{Cu}(1)$ site, which in turn leads to a less puckered plane. The oxygen $\text{O}(4)$ on the apical site shows the largest displacement, moving 0.09 \AA away from the dopant ion. Thus, the substitutional dopants cause small changes in the local symmetry. We should add that no significant movement from the undoped positions is found for nearest-neighbor barium and yttrium ions.

In Table II, the calculated $M^{2+}-\text{O}(4)$ bond distances together with the adjacent $\text{Cu}(1)-\text{O}(4)$ bond distances for the $3d$ dopant ions (M^{2+}) are summarized. In general, we observe a small change in the $\text{Cu}(1)-\text{O}(4)$ dis-

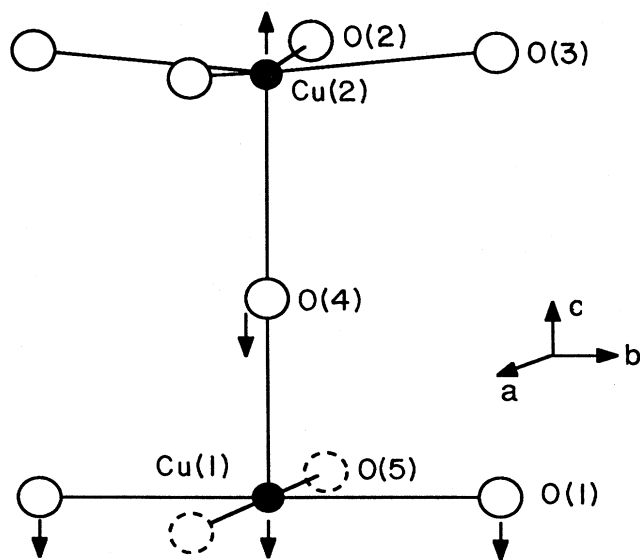


FIG. 3. Motion of ions near a divalent transition-metal ion substituting at the $\text{Cu}(2)$ plane site. Approximate displacements are as follows: $\text{Cu}(1)$ 0.07 \AA ; M^{2+} on $\text{Cu}(2)$ 0.05 \AA ; $\text{O}(1)$ 0.03 \AA ; $\text{O}(2)$ and $\text{O}(3)$ 0.002 \AA ; $\text{O}(4)$ 0.09 \AA .

TABLE II. Calculated bond distances (in \AA) for divalent dopant substitution on the $\text{Cu}(2)$ site.

M^{2+}	$M-\text{O}(4)$	$\text{Cu}(1)-\text{O}(4)$
Fe	2.4416	1.8430
Co	2.4500	1.8434
Ni	2.3469	1.8614
Cu^a	2.3095	1.8741
Zn	2.4275	1.8514

^aUndoped lattice.

tances, but a significant deviation for the distances between dopant ion and $\text{O}(4)$. From neutron powder-diffraction experiments,⁹ correlations of certain average bond lengths with T_c have been discussed. Therefore, to illustrate the behavior of our computed bond distances we plotted both the $M^{2+}-\text{O}(4)$ and the $\text{Cu}(1)-\text{O}(4)$ distances versus T_c , shown in Fig. 4. First, a trend towards

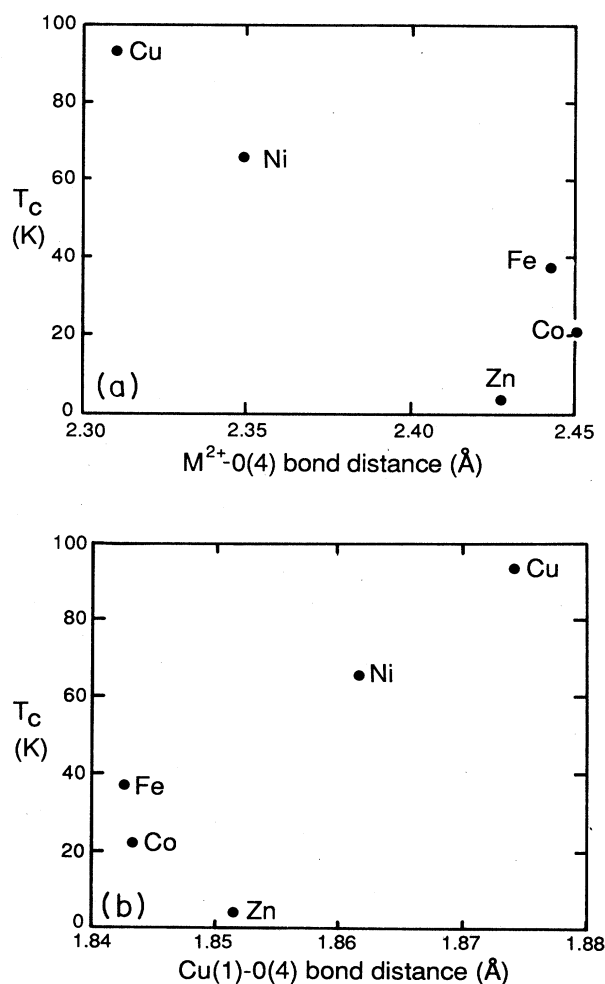
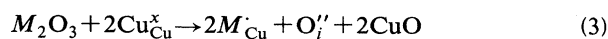


FIG. 4. (a) Plot of variation of T_c vs $M^{2+}-\text{O}(4)$ bond distance. (b) Plot of variation of T_c vs $\text{Cu}(1)-\text{O}(4)$ bond distance. Observed values of T_c are from Ref. 2.

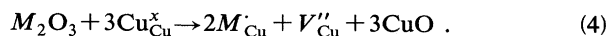
decreasing T_c with increasing M^{2+} —O(4) and decreasing Cu(1)—O(4) bond distances is found. We recognize, however, that the observed value of T_c is strongly dependent on the precise dopant concentration. Nonetheless, diffraction measurements⁹ have similarly found T_c decreasing systematically with decreasing Cu(1)—O(4) bond distance, for both the Co-doped and oxygen-deficient materials. It has been suggested that the Cu(1)—O(4) bond distance is an important parameter reflecting the local electronic properties.⁹ Our calculations are in accord with this picture and suggest that the depression in T_c is closely related to the local structural and electronic environment. Second, it is interesting to note that, even though Zn^{2+} has an ionic radius close to that of Cu^{2+} , a relatively large increase in the M^{2+} —O(4) bond distance is calculated [Fig. 4(a)]. Experimentally, Zn^{2+} is observed^{2,5,7,14} to have the most deleterious effect on T_c . In contrast we find the smallest change in the two bond distances considered, for the case of Ni^{2+} (Table II). We also note that T_c is suppressed markedly faster for Zn^{2+} (Ref. 14) than for Ni^{2+} (Ref. 13). For the latter case T_c drops fairly smoothly to 66 K after $x=0.20$ Ni substitution in $YBa_2(Cu_{1-x}M_x)_3O_7$, whereas T_c is below 10 K after only $x=0.05$ Zn substitution. Interestingly, since Cu^{2+} and Ni^{2+} have similar electronic properties and ionic radii, it has been speculated that high-temperature superconductivity might be found in analogous nickel-oxide materials.

Our previous study²⁶ of electronic defects in $YBa_2Cu_3O_7$ computed large polarization energies associated with the localized small polarons Cu^{3+} and O^- ; these energies indicate strong electron-lattice interactions. The interaction between the polarization fields of these polaronic species was subsequently investigated as a possible hole-coupling mechanism to form bipolarons. All the configurations considered²⁶ were found to be weakly unstable, with binding energies typically in the range 0.3–1.0 eV. As discussed by Catlow *et al.*²⁷ and deJongh,⁴⁰ it is possible that bipolarons may be stabilized when antiferromagnetic exchange energies and elastic strain terms are taken into account, to overcome the intersite Coulomb repulsion that opposes such pair formation. We have extended these calculations by testing the effect of nearest-neighbor $3d$ divalent dopant ions on the bipolaron binding energies. Our preliminary results³⁶ indicate insignificant change in the calculated binding energies. Therefore, these findings do not provide support for a small bipolaron model.

For trivalent impurities substituting at Cu^{2+} sites there are two alternative charge-compensating defects—oxygen interstitials or copper vacancies. The corresponding defect reactions are



or



The former process involving oxygen incorporation is calculated to have the lowest energy²⁶ and is, therefore, predicted to be the majority compensating mechanism.

This result is in accord with thermogravimetric measurements⁵ that show an increase in oxygen content with increasing Al^{3+} , Fe^{3+} , and Co^{3+} dopant concentration, and in particular finds that each added Co atom pulls in 0.5 oxygen atom. Note that oxygen uptake accounts for the observed⁵ increase in unit-cell volume even though Al^{3+} , Fe^{3+} , and Co^{3+} are all smaller than Cu^{2+} . We recall that the charge distribution in our potential model has assigned a $2+$ charge state to Cu(1). This model is consistent with a number of photoemission studies^{41–44} that indicate no Cu^{3+} in the ground state of $YBa_2Cu_3O_7$. Some discussions, however, have suggested that Cu(1) is in fact trivalent. It is tempting to claim that substitution of Cu^{3+} by trivalent dopants would not require charge compensation and, therefore, the increase in oxygen content would not be observed.

The calculated energies of solution for the trivalent ions Al, Sc, Fe, Ga, and Bi are presented in Table III and displayed graphically in Fig. 2(b). Examination of these energies reveals that the trivalent dopants are predicted to favor substitution at the Cu(2) site. The computed solution energies for Al^{3+} , Sc^{3+} , and Fe^{3+} are exothermic. However, ΔE for Bi^{3+} substitution is sufficiently high to allow this process to be eliminated. Our predicted preference for the plane site does not accord with x-ray and neutron-diffraction analyses,^{4,5} which suggest that Al impurities occupy the chain site. In addition, extended x-ray-absorption fine-structure (EXAFS) data¹² suggest that Fe occupies distorted Cu(1) sites with a small occupation of the Cu(2) site. This latter study¹² also found evidence for association of dopant atoms into chains along the $\langle 110 \rangle$ direction, indicating a type of Fe-Fe short-range ordering. According to Mössbauer experiments,^{5,16} the Fe dopant is distributed over both copper sites, but substitutes predominantly for Cu(1). However, there has been considerable debate concerning the site assignment of the observed quadrupole doublets and isomer shifts for ^{57}Fe in $YBa_2Cu_3O_7$.

The entries in Table III represent two extreme cases of localization of the trivalent impurity with the compensating oxygen interstitial ion. We consider two neighboring impurity ions on the Cu(1) chain site, adjacent to the interstitial oxygen ion in one case. In the other case the impurity ions in the plane are separated from the interstitial oxygen ion. Our calculations indicate that the lattice polarization and ion relaxation favor the separated model. These calculations do not address chemical effects such as whether the coordination ligands are sufficient to maintain a particular oxidation state of the impurity. Thus we

TABLE III. Calculated energies of solution (in eV per dopant ion) for trivalent cation substitution for copper.

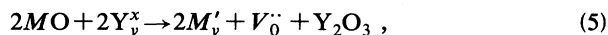
M_2O_3	$M_2O_3 + 2Cu_{Cu}^x = 2M'_{Cu} + O''_i + 2CuO$	
	$\Delta E_{Cu(1)}$	$\Delta E_{Cu(2)}$
Al_2O_3	0.10	−1.66
Sc_2O_3	0.75	−1.44
Fe_2O_3	−0.31	−1.84
Ga_2O_3	−0.25	NC ^a
Bi_2O_3	4.23	4.22

^aCalculation not converged.

must use the calculations in relation to experiments in order to distinguish which of the two extreme cases is operative. It is important to add, however, that when the more localized model is considered, the dopants are predicted to favor the chain site. Finally, since an increase in oxygen content is predicted to result from trivalent dopants on the copper sublattice, it seems likely that this, together with the related effect of oxygen (dis)ordering, are important factors in the suppression of superconductivity in $\text{YBa}_2\text{Cu}_3\text{O}_7$.

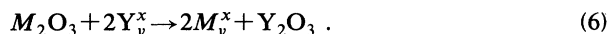
B. Substitution for yttrium

Incorporation of divalent ions into the yttrium-based lattice can be represented by the defect equation



with extrinsic oxygen vacancies being created to preserve charge neutrality. The calculated energies of solution, reported in Table IV, are high and positive, suggesting that the levels of these divalent impurities on yttrium sites will be negligible even at high temperatures, as expected. Interestingly, the plot of ΔE versus ionic radius, in Fig. 5(a), shows an energy minimum close to the ionic radius of Y^{3+} ($r = 0.90 \text{ \AA}$).

In the case of rare-earth substitution for Y^{3+} , the appropriate defect equation is



Examination of Table V and Fig. 5(b) again reveals a strong correlation between the solution energies and the size of the dopant, with ΔE increasing smoothly with increasing ionic radius. These findings are consistent with Raman spectra¹⁵ for the fully substituted systems, $\text{RBa}_2\text{O}_3\text{O}_7$, that observe modes attributed to $\text{Cu}(1)\text{--O}(4)$ and $\text{Cu}(2)\text{--O}(2,3)$ vibrations, exhibiting highly correlated variations in vibrational frequency with ionic radius.

The calculated energies change by approximately 20% from Lu^{3+} , which has the smallest radius, to La^{3+} , which has the largest. The highest value is computed to La_2O_3 ; a result that is compatible with the observation¹⁸ that among the trivalent rare-earth ions La^{3+} is the most difficult to substitute for Y^{3+} . In fact, diffraction studies^{8,19} have found that La^{3+} is partially substituting for Ba^{2+} . This observation is not surprising considering the

TABLE IV. Calculated energies of solution (in eV per dopant ion) for divalent cation substitution for yttrium.

MO	ΔE
MgO	8.29
CaO	7.12
SrO	12.89
FeO	7.87
CoO	8.14
NiO	5.51
ZnO	5.50
CdO	5.33

TABLE V. Calculated energies of solution (in eV per dopant ion) for trivalent cation substitution for yttrium.

M_2O_3	ΔE
La_2O_3	3.53
Nd_2O_3	3.21
Eu_2O_3	3.05
Gd_2O_3	3.03
Ho_2O_3	2.91
Lu_2O_3	2.91

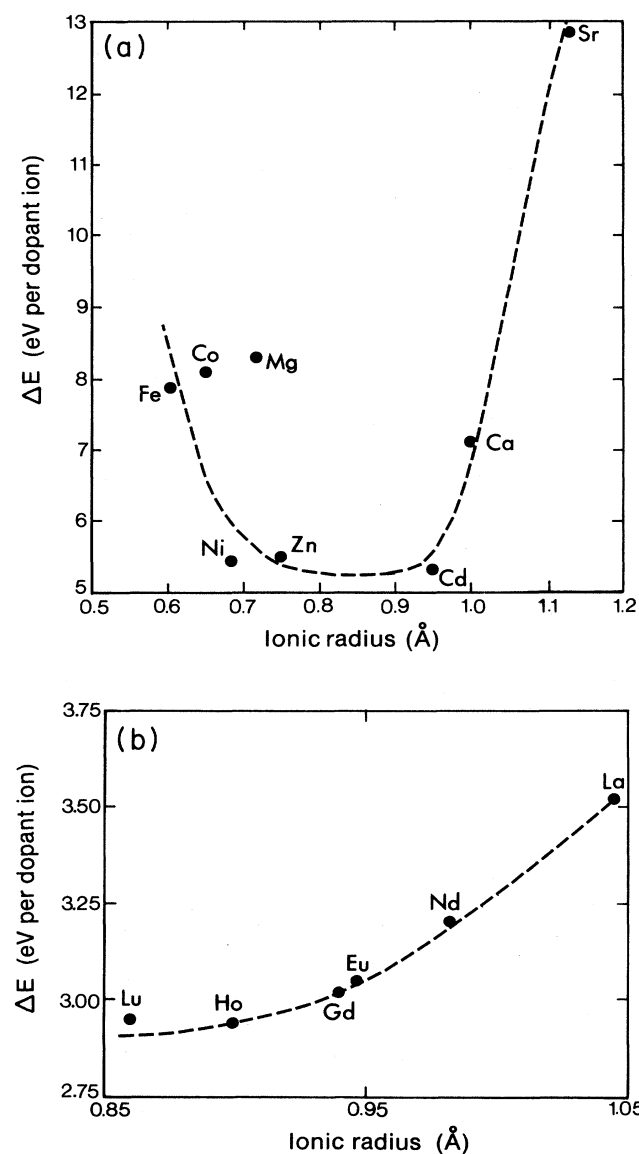


FIG. 5. Calculated energies of solution as a function of dopant ion radius for yttrium substitution (a) divalent ions, (b) trivalent rare-earth ions.

size of La^{3+} ($r=1.06 \text{ \AA}$), which is both the largest in the rare-earth series and intermediate between that of Y^{3+} ($r=0.90 \text{ \AA}$) and Ba^{2+} ($r=1.36 \text{ \AA}$). We note, however, that the magnitudes of ΔE for all the rare-earth oxides are high. These results suggest that the levels of rare-earth dopant on the yttrium sublattice will be low, unless stabilization due to clustering occurs at higher dopant concentrations. Further, the solution energies listed in Table V are energetically unfavorable in comparison with the corresponding values for substitution on the barium site (Table VII). Our calculations, therefore, predict site preference for the latter, a point to which we return later.

C. Substitution for barium

The defect reaction for the dissolution of divalent ions onto the barium sublattice is



The calculated energies of solution are reported in Table VI and plotted versus ionic radius in Fig. 6(a). Once again a trend between ΔE and ion size is evident. Experimentally, Dou *et al.*^{17(a)} have suggested a linear relationship between T_c and the ionic radius of alkaline-earth dopants on the barium site. In general, our calculations predict that the 3d elements substitute site selectively for copper, whereas the larger alkaline-earth dopants, Ca^{2+} and Sr^{2+} , substitute for barium. These results are not surprising when considering that the ion size and orbital structure of the divalent 3d ions are close to that of Cu^{2+} . From our analysis of ion positions after relaxation, we find large displacements (Ca 0.4 \AA) of the substituting alkaline-earth cations, along the c axis towards the copper-oxygen plane and away from the Cu(1) chain. The off-center position is stabilized by the resulting polarization energy of the lattice.²³ A summary of the calculated Cu—O(4) and M —O(4) bond distances, in the vicinity of the alkaline-earth dopant ion, are given in Table VIII and plotted versus ionic radius in Fig. 7. The main effect of alkaline-earth substitution is to change the Cu(2)—O(4) distance, which becomes shorter with decreasing ion size. By comparison, the Cu(1)—O(4) distance remains almost constant across the series. Furthermore, apart from Mg^{2+} and M —O(4) distance also remains close to the undoped lattice value. As expected,

TABLE VI. Calculated energies of solution (in eV per dopant ion) for divalent cation substitution for barium.

$MO + \text{Ba}_{\text{Ba}}^x = M_{\text{Ba}}^x + \text{BaO}$	
MO	ΔE
MgO	2.49
CaO	1.03
SrO	0.97
FeO	2.10
CoO	2.07
NiO	2.43
ZnO	2.30
CdO	1.34

TABLE VII. Calculated energies of solution (in eV per dopant ion) for trivalent cation substitution for barium.

$M_2\text{O}_3 + \text{Ba}_{\text{Ba}}^x = 2M_{\text{Ba}}^x + \text{O}_i' + 2\text{BaO}$	
$M_2\text{O}_3$	ΔE
La_2O_3	0.98
Nd_2O_3	1.11
Eu_2O_3	1.22
Gd_2O_3	1.30
Ho_2O_3	1.45
Lu_2O_3	1.66

the largest deviation is for Mg^{2+} , owing to the large difference in ionic radii between the substitutional and host cations. It is interesting to note that the solution energy for Mg^{2+} substitution for Ba^{2+} is unfavorable, and

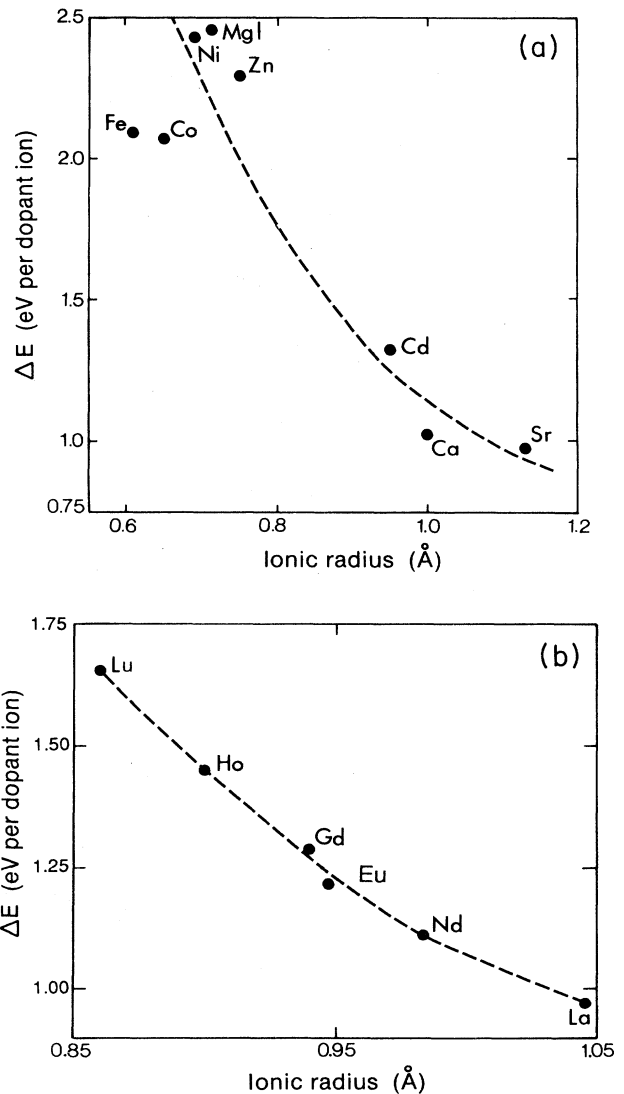


FIG. 6. Calculated energies of solution as a function of dopant ion radius for barium substitution (a) divalent ions, (b) trivalent rare-earth ions.

TABLE VIII. Calculated bond distances (in Å) for alkaline-earth substitution on the barium site.

M^{2+}	$M-O(4)$	$Cu(1)-O(4)$	$Cu(2)-O(4)$
Ba ^a	2.7305	1.8741	2.3095
Sr	2.7653	1.8805	2.1727
Ca	2.7728	1.8844	2.1183
Mg	3.0025	1.8814	2.0531

^aUndoped lattice.

is in fact predicted to dissolve in the crystal at the copper site. The trends exhibited in Fig. 7 therefore suggest that the smaller size of these cations perturbs the local structure, causing a slight disruption in the copper-oxygen plane substructure near the barium site. This behavior could explain the observed changes in superconducting properties, although it is unclear whether structural changes are directly linked to the reduction in T_c . Indeed, an alternative explanation has recently been proposed⁴⁵ in terms of the polarizability of the Ba^{2+} and Sr^{2+} ions. Ronay and Newns⁴⁵ suggest that the small change in T_c with alkaline-earth substitution is due to a "polarizability shift," which affects the two-hole coupling mechanism.

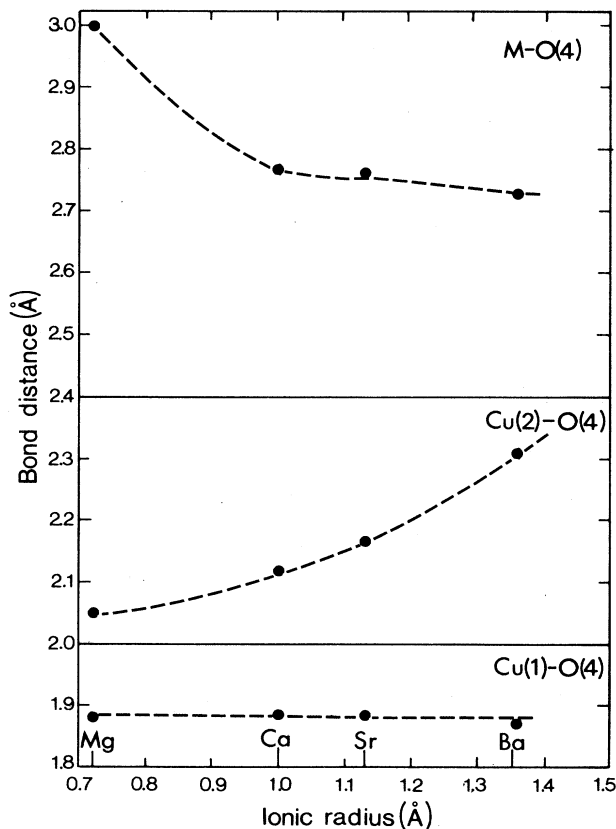
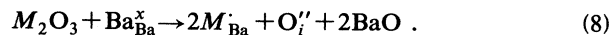


FIG. 7. Calculated $M-O(4)$, $Cu(1)-O(4)$, and $Cu(2)-O(4)$ bond distances vs M^{2+} ionic radius, where M denotes alkaline earth.

For rare-earth substitution of barium we find an increase in the oxygen content to be the most favorable mode of charge compensation, as opposed to a reduction in the formal copper valence



Again, a correlation with ion size is observed, similar to the behavior on the yttrium site, although in this case La^{3+} has the lowest solution energy [Fig. 6(b)]. As noted earlier, examination of the solution energies in Tables V and VII indicates that for these rare-earth oxides, isolated cation substitution at the barium site is energetically favored over the yttrium site in $YBa_2Cu_3O_7$. This would consequently lead to incorporation of additional oxygen into the structure, with increasing rare-earth concentration, at a predicted rate of 0.5 oxygen-dopant ion, from Eq. (8). Solid solutions of the system $R(Ba_{2-x}R_x)Cu_3O_{7+\delta}$ have been investigated¹⁰ and the findings discussed in terms of an ion size argument. Our results similarly suggest that dissolution is largely dependent on ion size, being most favorable for La^{3+} and becoming more difficult with decreasing ionic radius. This behavior accords with experiment,¹⁰ which finds the solubility limits on the barium sublattice decreasing in the order La, Nd, Sm, Eu, Gd to Dy. Note that the rare-earth ions towards the Lu end of the lanthanide series are comparable in size to Y^{3+} ($r=0.90$ Å), and a degree of mixing among the yttrium and barium sites might be expected to occur.

In conclusion, we have shown that the application of atomistic simulation techniques can provide a useful systematic treatment of dopant phenomena in the $YBa_2Cu_3O_7$ ceramic oxide. While there may remain some uncertainties in the calculated solution energies for this complex system, our study clearly demonstrates the ability of the method to distinguish between alternative modes of dopant substitution and compensation mechanisms. The results discussed in this paper have first indicated the importance of ion size effects in the site-selective occupancy of dopant ions. The calculations have produced trends as a function of ionic radius that are generally consistent with the available experimental data. These findings indicate the sensitivity of the interatomic potentials to small change in ion size and provide support for the general validity of the methods used. It is worth noting that we have not employed unrelated procedures for parameter mixing, but transferred potentials for the dopant ion interactions from corresponding binary oxides. From our analysis of local ion displacements immediately surrounding the dopant ion, we find a trend towards decreasing T_c with increasing $M^{2+}-O(4)$ (where $M=Fe, Co, Ni, Cu,$ and Zn) and decreasing $Cu(1)-O(4)$ bond distances. This picture is consistent with neutron-diffraction measurements⁹ that have similarly shown T_c decreasing with decreasing $Cu(1)-O(4)$ bond distance, for Co-doped and oxygen-deficient $YBa_2Cu_3O_{7-\delta}$. Our study, therefore, suggests that the superconducting properties are closely related to the local structural and electronic environment. From the calculated energies of solution, substitution at the $Cu(2)$

plane site emerged as the most probable mode of substitution for divalent $3d$ cations such as Ni^{2+} and Zn^{2+} , whereas the alkaline-earth dopants Ca^{2+} and Sr^{2+} would selectively substitute for barium, in agreement with experiment. Contrary to common models, it is predicted that Al^{3+} and Fe^{3+} dissolve in the crystal preferentially at Cu(2). This can be rationalized in terms of our discussion dealing with two extreme cases of localization of the trivalent dopant and the compensating oxygen interstitial ion. It is important to add, however, that if a more localized model is operative, the Cu(1) site would be favored. Nevertheless, our results indicate an increase in oxygen content with increasing trivalent ion concentration, as is observed experimentally. Finally, the calculations suggest that substitution of rare-earth ions is energetically

most favorable at the barium site, in particular for La^{3+} . Note that in this study we have considered systems at high dilution. At higher dopant concentrations, however, the association of dopants or their charge-compensating defects with the possibility of long-range ordering or the formation of clusters may play an increasingly crucial role in defect stabilization and hence in the effective solution energies that are computed. These defect interactions obviously are subjects for further study.

ACKNOWLEDGMENTS

We are grateful to José Mir and Mark Lelental for helpful discussions.

*Permanent address: Department of Chemistry, University of Surrey, Guildford, Surrey GU2 5XH, UK.

- ¹P. H. Hor, R. L. Meng, Y. Q. Wang, L. Gao, Z. J. Huang, J. Bechtold, K. Forster, and C. W. Chu, *Phys. Rev. Lett.* **58**, 1891 (1987).
- ²G. Xiao, F. H. Streitz, A. Garvin, Y. W. Du, and C. L. Chien, *Phys. Rev. B* **35**, 8782 (1987).
- ³Y. Maeno, T. Tomita, M. Kyogoku, S. Awaji, Y. Aoki, K. Hosino, A. Minami, and T. Fujita, *Nature* **328**, 512 (1987).
- ⁴T. Siegrist, L. F. Schneemeyer, J. V. Waszczak, N. P. Singh, R. L. Opila, B. Batlogg, L. W. Rupp, and D. W. Murphy, *Phys. Rev. B* **36**, 8365 (1987).
- ⁵J. M. Tarascon, P. Barboux, P. F. Miceli, L. H. Greene, G. W. Hull, M. Eibschutz, and S. A. Sunshine, *Phys. Rev. B* **37**, 7458 (1988).
- ⁶J. Jung, J. P. Frank, W. A. Miner, and M. A.-K. Mohammed, *Phys. Rev. B* **37**, 7510 (1988).
- ⁷E. Takayama-Muromachi, Y. Uchida, and K. Kato, *Jpn. J. Appl. Phys.* **26**, L2087 (1987).
- ⁸R. J. Cava, B. Batlogg, R. M. Fleming, S. A. Sunshine, A. Ramirez, E. A. Rietman, S. M. Zahurak, and R. B. van Dover, *Phys. Rev. B* **37**, 5912 (1988).
- ⁹P. F. Miceli, J. M. Tarascon, L. H. Greene, P. Barboux, F. J. Rotella, and J. D. Jorgensen, *Phys. Rev. B* **37**, 5932 (1988).
- ¹⁰K. Zhang, B. Dabrowski, C. U. Segre, D. G. Hinks, I. K. Schuller, J. D. Jorgensen, and M. Slaski, *J. Phys. C* **20**, L935 (1987).
- ¹¹B. D. Dunlap, J. D. Jorgensen, W. K. Kwok, C. W. Kimball, J. L. Matykievicz, H. Lee, and C. U. Segre, *Physica C* **153-155**, 1100 (1988).
- ¹²J. B. Boyce, F. Bridges, T. Claeson, R. S. Howland, T. H. Geballe, and M. Nygren, *Physica C* **153-155**, 852 (1988); F. Bridges, J. B. Boyce, T. Claeson, T. H. Geballe, and J. M. Tarascon, *Phys. Rev. B* **39**, 11 603 (1989).
- ¹³J. F. Bringley, T. M. Chen, B. A. Averill, K. M. Wong, and S. J. Poon, *Phys. Rev. B* **38**, 2432 (1988).
- ¹⁴B. Jayaram, S. K. Agarwal, C. V. N. Rao, and A. V. Narlikar, *Phys. Rev. B* **38**, 2903 (1988).
- ¹⁵H. J. Rosen, R. M. Macfarlane, E. M. Engler, V. Y. Lee, and R. D. Jacowitz, *Phys. Rev. B* **38**, 2460 (1988).
- ¹⁶I. Nowik, M. Kowitz, I. Felner, and E. R. Bauminger, *Phys. Rev. B* **38**, 6677 (1988).
- ¹⁷(a) S. X. Dou, A. J. Bourdillon, X. Y. Sun, H. K. Liu, J. P. Zhou, N. Savvides, C. C. Sorrell, and K. E. Easterling, *Phys. Status Solidi B* **147**, K153 (1988); (b) B. W. Veal, W. K. Kwok, A. Umezawa, G. W. Crabtree, J. D. Jorgensen, J. W. Downey, L. J. Nowicki, A. W. Mitchell, A. P. Paulikas, and C. H. Sowers, *Appl. Phys. Lett.* **51**, 279 (1987).
- ¹⁸S. Katano, S. Funahashi, T. Hatano, A. Matsushita, K. Nakamura, T. Matsumoto, and K. Ogawa, *Jpn. J. Appl. Phys.* **26**, L1046 (1987).
- ¹⁹C. U. Segre, B. Dabrowski, D. G. Hinks, K. Zhang, J. D. Jorgensen, M. A. Beno, and I. K. Schuller, *Nature* **329**, 227 (1987).
- ²⁰F. Beech, S. Miraglia, A. Santoro, and R. S. Roth, *Phys. Rev. B* **35**, 8778 (1987).
- ²¹M. A. Beno, L. Soderholm, S. W. Capone II, D. G. Hinks, J. D. Jorgensen, I. K. Schuller, C. U. Segre, K. Zhang, and J. D. Grace, *Appl. Phys. Lett.* **50**, 1688 (1987).
- ²²J. J. Capponi, C. Chaillout, A. W. Hewat, P. Lejay, M. Magezio, N. Nguyen, B. Raveau, J. L. Souberroux, J. L. Tholence, and R. Tournier, *Europhys. Lett.* **3**, 1301 (1987).
- ²³C. R. A. Catlow, in *Computer Simulation of Solids*, Vol. 166 of *Lecture Notes in Physics*, edited by C. R. A. Catlow and W. C. Mackrodt (Springer-Verlag, Berlin, 1982).
- ²⁴C. R. A. Catlow, *Annu. Rev. Mater. Sci.* **16**, 517 (1986).
- ²⁵C. R. A. Catlow, in *Solid-State Chemistry: Techniques*, edited by A. K. Cheetham and P. Day (Clarendon, Oxford, 1987), Chap. 7.
- ²⁶R. C. Baetzold, *Phys. Rev. B* **38**, 11 304 (1988).
- ²⁷M. S. Islam, M. Leslie, S. M. Tomlinson, and C. R. A. Catlow, *J. Phys. C* **21**, L109 (1988); C. R. A. Catlow, S. M. Tomlinson, M. S. Islam, and M. Leslie, *ibid.* **21**, L1085 (1988).
- ²⁸B. G. Dick and A. W. Overhauser, *Phys. Rev.* **112**, 90 (1958).
- ²⁹N. F. Mott and M. J. Littleton, *Trans. Faraday Soc.* **34**, 485 (1938).
- ³⁰M. Leslie, *Solid State Ionics* **8**, 243 (1983); Science and Engineering Research Council, Daresbury Laboratory Report No. DL/SCI/TM31T, 1982 (unpublished).
- ³¹M. J. Norgett, Atomic Energy Research Establishment, Harwell Report No. R7650, 1974 (unpublished).
- ³²G. V. Lewis and C. R. A. Catlow, *J. Phys. Chem. Solids* **47**, 89 (1986); *J. Phys. C* **18**, 1149 (1985).
- ³³C. R. A. Catlow, R. James, W. C. Mackrodt, and R. F. Stewart, *Phys. Rev. B* **25**, 1106 (1982).
- ³⁴C. S. Vempati and P. W. M. Jacobs, *Cryst. Lattice Defects Amorph. Mater.* **10**, 9 (1983).
- ³⁵C. R. A. Catlow, C. M. Freeman, M. S. Islam, R. A. Jackson, M. Leslie, and S. M. Tomlinson, *Philos. Mag.* **A58**, 123 (1988).

- ³⁶R. C. Baetzold and M. S. Islam (unpublished).
- ³⁷C. R. A. Catlow and A. M. Stoneham, *J. Phys. C* **16**, 4321 (1983).
- ³⁸A. M. Stoneham and J. R. Harding, *Annu. Rev. Phys. Chem.* **37**, 53 (1986).
- ³⁹F. A. Kroger and H. J. Vink, *Solid State Phys.* **3**, 307 (1956).
- ⁴⁰L. J. deJongh, *Physica C* **152**, 171 (1988); *J. Chim. Phys.* **85**, 1105 (1988).
- ⁴¹J. A. Yarmoff, D. R. Clarke, W. Drube, U. O. Karlsson, A. Taleb-Ibrahimi, and F. J. Himpsel, *Phys. Rev. B* **36**, 3967 (1987).
- ⁴²S. Horn, J. Cai, S. A. Shaheen, Y. Jeon, M. Croft, C. L. Chang, and M. L. denBoer, *Phys. Rev. B* **36**, 3985 (1987).
- ⁴³A. Fujimore, E. Takayami-Muromachi, and Y. Uchida, *Solid State Commun.* **63**, 857 (1987).
- ⁴⁴T. Iwazumi, I. Nakai, M. Izumi, H. Oyanagi, H. Sawada, H. Ikeda, Y. Saito, Y. Abe, K. Takita, and R. Yoshizaki, *Solid State Commun.* **65**, 213 (1988).
- ⁴⁵M. Ronay and D. M. Newns, *Phys. Rev. B* **39**, 9 (1989).